Alkaline cavities and tetrahedra in $Rb_xCs_{2-x}ZnCl_4$ and $K_xCs_{2-x}ZnCl_4$ solid solutions

1997 J. Phys.: Condens. Matter 9 825

(http://iopscience.iop.org/0953-8984/9/4/004)

J. Phys.: Condens. Matter **9** (1997) 825–843. Printed in the UK PII: S0953-8984(97)76846-2

Alkaline cavities and tetrahedra in $Rb_xCs_{2-x}ZnCl_4$ and $K_xCs_{2-x}ZnCl_4$ solid solutions

C Kolinsky†‡, M Jannin†, R Puget†, P Delarue† and G Godefroy†

† Laboratoire de Physique de l'Université de Bourgogne, URA 1796 CNRS, Faculté des Sciences Mirande, BP138, 21004 Dijon Cédex, France

‡ Equipe de Thermophysique de la Matiére Condensée, Laboratoire de Dynamique et Structure des Matériaux Moléculaires, URA CNRS 801, Université du Littoral Quai Freycinet 1, BP 5526, 59739 Dunkerque Cédex 1, France

Received 31 July 1996, in final form 8 November 1996

Abstract. Seven different $Rb_xCs_{2-x}ZnCl_4$ crystals were grown with $0 < x < 2$ while seven different $K_xCs_{2-x}ZnCl_4$ crystals were grown with $0 < x \leqslant 1$, the limit value $x = 1$ corresponding to the clearly defined $KCsZnCl_4$ compound. A crystallographic study of these solid solutions was performed by comparison with the pure Cs_2ZnCl_4 crystal. Structures were solved in the *Pnma* space group for the rubidium solid solutions and in the $P2_12_12_1$ space group for the potassium ones. It was shown that the distribution of Cs and Rb, or Cs and K, among the two cationic sites called A_1 and A_2 was not random: Rb and K exhibit a higher affinity for the smallest cavity, the A_2 site. While the phase transition of Rb_2ZnCl_4 and K_2ZnCl_4 can be interpreted as rotations of the rigid $ZnCl_4$ tetrahedra mainly around the $\boldsymbol{a}$ direction, the substitution of Cs by Rb or K not only supplies the $\boldsymbol{a}$ rotation of $ZnCl_4$ tetrahedra but, as shown by a first-order approximation model, also changes their size and shape.

1. Introduction

Potassium tetrachlorozincate K_2ZnCl_4 undergoes the classical phase sequence for the A_2BX_4 compounds: starting from the normal paraelectric orthorhombic high-temperature phase (N) (space group *Pnma*), the crystal transforms to an incommensurate phase (INC) at $T_i = 553$ K [1, 2]. In the incommensurate phase, the crystal lattice is modulated along the a direction with the wave number modulation vector $\boldsymbol{q} = (1/3 - \delta)\boldsymbol{a}_0$, where $\boldsymbol{a}_0$ represents the reciprocal lattice parameter of the normal phase. The commensurate ferroelectric phase (C) (space group $Pn2_1a$ at $T_c = 403$ K [3] is caused by the lock-in of $\boldsymbol{q}$ at the commensurate value $\boldsymbol{q} = 1/3\boldsymbol{a}_0$. Thus, the unit cell is tripled along the a axis. Recent studies displayed other phase transitions around $T_1 = 250$ K and 145 K [4, 5]. Rubidium tetrachlorozincate Rb_2ZnCl_4 exhibits the same phase transitions but with lower transition temperatures: $T_i = 302$ K, $T_c = 189$ K [6, 7] and $T_l = 75$ K [8–11]. On the other hand, caesium tetrachlorozincate Cs_2ZnCl_4 does not exhibit any phase transition: at each temperature it belongs to the normal paraelectric phase (space group *Pnma*).

The crystal structures of each phase of these three compounds have been widely studied by x-ray neutron diffraction and other methods. For example, see [12–15] for K_2ZnCl_4 [16–18] for Rb_2ZnCl_4 and [19] Cs_2ZnCl_4.

0953-8984/97/040825+19$19.50

The lattice structure of the normal phase (space group *Pnma*) consists of four symmetry-related groups of one $ZnCl_4$ tetrahedron and two alkaline atoms (Cs, Rb or K). As an example, the projection along the *c* axis of the Cs_2ZnCl_4 structure is presented in figure 1(a). Each atom is in a special position except for the equivalent chlorine atoms Cl_3 and Cl_4 which are in a general position. The Cs_1 and Cs_2 cations can occupy two crystallographically non-equivalent sites, labelled A_1 and A_2. Another projection given in figure 1(b) shows that the normal phase structure can also be described as the juxtaposition of two parallel chain types. The caesium cations situated in the A_1 site build up an alternating linear chain (usually labelled as β) with the tetrahedra: $\ldots Cs^+(ZnCl_4)^{2-}Cs^+\ldots$ parallel to the *a* axis. The second chain (α) consists solely of caesium positioned in the A_2 site. This zig-zag chain, $\ldots Cs^+$–$Cs^+\ldots$, is situated in a symmetry plane, parallel to the *a* direction, and its average position corresponds to the position of the pseudo-hexagonal *a* axis of the A_2BX_4 type structure.

The instability presented by these compounds is interpreted as rotations of rigid $ZnCl_4$ tetrahedra, which are the most voluminous entities of the structure [17]. The existence of an incommensurate lattice instability, or its absence for $CsZnCl_4$, depends basically on the effective volume of the alkaline cation compared with the size of the $ZnCl_4$ tetrahedra [20]. The latter can be compared to rigid and undistorted entities. If they are sufficiently free, the structure is stable; if they are compressed in the normal phase, the structure is unstable and a transition is observed when the temperature decreases.

In order to obtain a better insight into the transition mechanism of the A_2ZnCl_4 materials, we decided to vary some stability parameters. Thus, we synthesized solid solutions composed of the same tetrahedron $ZnCl_4$, and one cation with increasing atomic radii: K^+, Rb^+ and C^+. We performed a systematic structural study of several $Rb_xCs_{2-x}ZnCl_4$ and $K_xCs_{2-x}ZnCl_4$ compounds. The structural data permitted us to obtain information on the occupation probability in host sites and on the behaviour of $ZnCl_4$ tetrahedra in mixed compounds.

Experimental details are presented in section 2. Subsection 3.1 is devoted to the structural determination of the two types of mixed compound. finally, subsection 3.2 is related to the phase transition mechanism study for our compounds. This study used the thermal agitation of the $ZnCl_4$ tetrahedra and the static deviations of these tetrahedra from their position in Cs_2ZnCl_4.

2. Experimental details

2.1. Sample preparations

Homogeneous composition in the whole crystal is the essential condition that allows the study of the alkaline cation distribution in our mixed compounds. The monocrystals we have used were grown by the procedure described by Arend *et al* [21] based on a temperature difference growth with thermally enforced convention and the use of saturated solutions in equilibrium with precipited solid phase. This method enables us to maintain a constant concentration of solution around the crystal during the whole growth process. Two different growth methods provided us with two kinds of sample:

(i) small samples of about $0.3 \times 0.3 \times 0.3$ mm^3 for the radiocrystallographic studies;
(ii) bigger samples (1 or 2 cm^3) for the dielectric measurements.

$Rb_xCs_{2-x}ZnCl_4$ crystals were all grown in the same conditions: $T = 313$ K, $\Delta T = 3$ K.

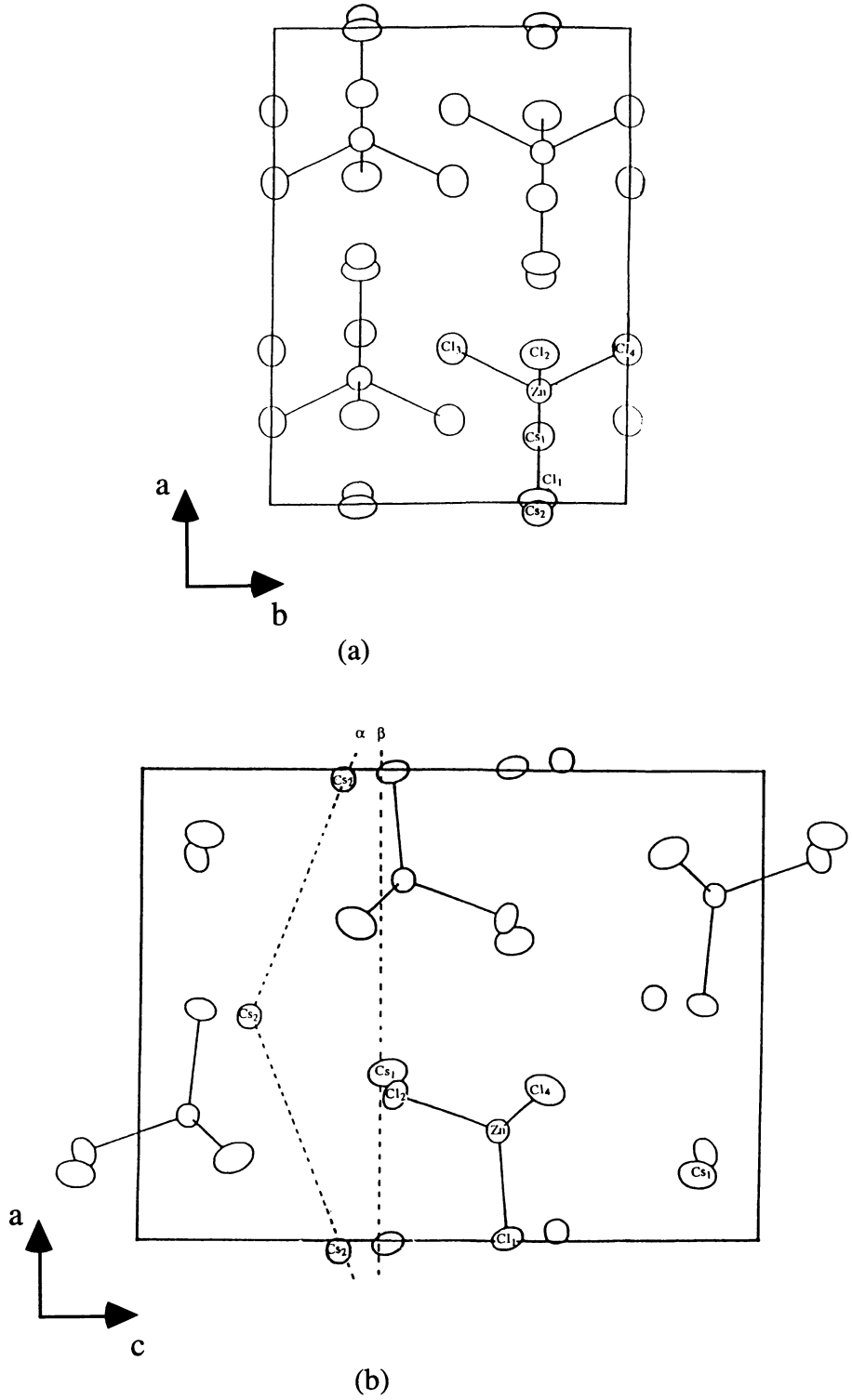

Figure 1. The crystal structure of Cs_2ZnCl_4 viewed along (a) the *c* axis and (b) the *b* axis.

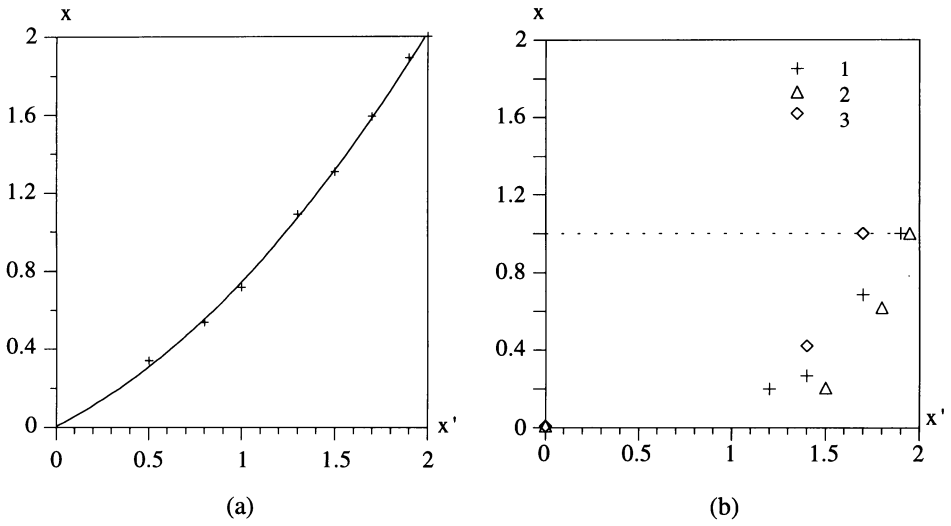

Figure 2. The experimental dependence of x in the crystal on x' in the mother solution for (a) the $Rb_xCs_{2-x}ZnCl_4$ mixed crystals and (b) the $K_xCs_{2-x}ZnCl_4$ mixed crystals.

The supersaturated solutions were obtained by dissolving weighed amounts of RbCl, CsCl and $ZnCl_2$ in a constant volume of warm water (molar ratio $x : 2 - x : 1$). For the $K_xCs_{2-x}ZnCl_4$ crystals, we replaced RbCl with KCl and the temperature conditions were $T = 293$ K, $\Delta T = 3$ K.

The composition of the mother solution was different of that of the mixed crystals, and analysis was necessary for each $Rb_xCs_{2-x}ZnCl_4$ or $K_xCs_{2-x}ZnCl_4$ crystal we studied. The chemical analysis, using atomic emission spectroscopy, was performed for each composition. The results were compared at the end of each structure refinement by comparison with the x value calculated from the occupation probabilities of K, Rb or Cs in the two cationic sites of the structure defined above. The results obtained by the two methods are in good agreement.

2.1.1. $Rb_xCs_{2-x}ZnCl_4$ compounds. Seven samples were synthesized corresponding to (1) $x = 0.34$, (2) $x = 0.54$, (3) $x = 0.71$, (4) $x = 1.11$, (5) $x = 1.31$, (6) $x = 1.59$ and (7) $x = 1.89$.

Figure 2 shows the correspondence between x and x' defined in the crystal and in the mother solution respectively.

2.1.2. $K_xCs_{2-x}ZnCl_4$ compounds. Crystals with seven different concentrations were also grown but with $0 < x \leqslant 1$: (1′) $x = 0.22$, (2′) $x = 0.27$, (3′) $x = 0.43$, (4′) $x = 0.62$, (5′) $x = 0.70$, (6′) $x = 0.85$ and (7′) $x = 1.00$.

Several series of crystallizations were performed. Figure 2 gives the experimental dependence of x on x'. Data are shown for three different crystallizations labelled 1–3, for which the process was slightly different. Only compounds with $0 < x \leqslant 1$ can be elaborated. When the potassium concentration increases in the solution up to $x' = 1.995$, we obtain crystals with a limit composition $KCsZnCl_4$.

2.2. Characterization measurements

2.2.1. Calorimetric experiments. Calorimetric measurements were performed on a Perkin–Elmer DSC-7 differential scanning calorimeter at a scanning speed of 10 K min^{-1} on cooling/heating. For all experiments, the sample, about 10 and 80 mg, was hermetically sealed in metal capsules.

2.2.2. X-ray experiments. The pattern of Bragg reflections was recorded at room temperature, measured by the precession method with Cu Kα radiation. This allowed us to check the quality of the sample and the absence of the incommensurate phase.

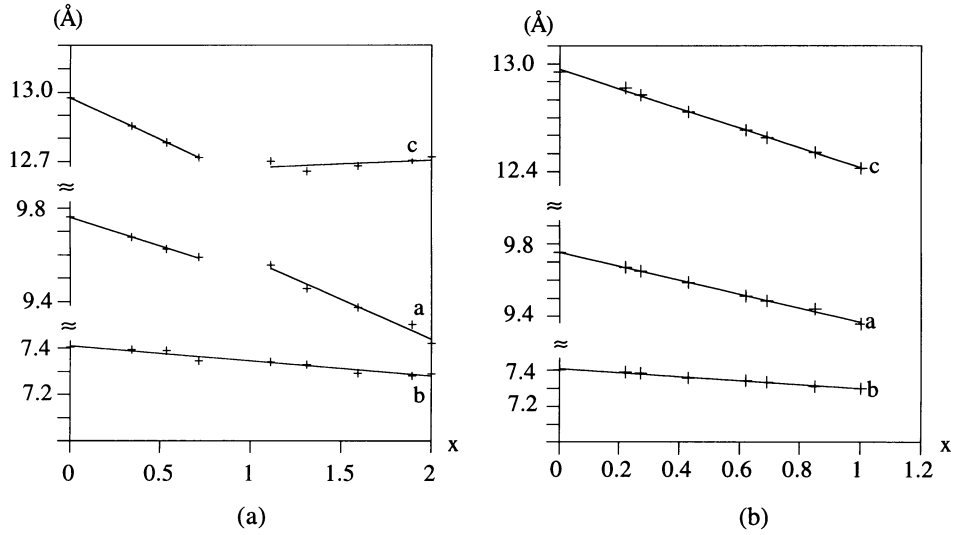

Figure 3. Evolution of the cell parameters versus the composition x in (a) the $Rb_xCs_{2-x}ZnCl_4$ mixed crystals (for $x = 2$, the results are referred to [18]) and (b) the $K_xCs_{2-x}ZnCl_4$ mixed crystals.

Data for structure determination were collected on an Enraf–Nonius four-circle diffractometer with monochromatized Mo Kα radiation ($\lambda = 0.710\,73$ Å; graphite monochromator), using a microVAX 3100 computer. Lattice parameters were refined from setting angles of 25 reflections in the $8^\circ < \theta < 15^\circ$ range. About 7000 reflections with $1^\circ < \theta < 30^\circ$ were collected using the $\omega/2\theta$ scan technique. During each data collection, three standard reflections were measured at 2 h intervals to verify that the intensity variation was negligible. The data were reduced and corrected for Lorentz and polarization effects, with semi-empirical absorption corrections, using the MolEN [22] programs. They were also used for resolutions and refinements of the structures. An improvement of the MolEN programs permitted us to refine the occupation probability in host sites. In fact, a new refined parameter was introduced in the basic programs. This parameter is the occupation probability, at one site, for caesium, rubidium or potassium ions. In practice, only one multiplicity is refined; the second one is deducted so that the sum at one site is constant and equal to one. Obviously, the multiplicity of each cation (K, Cs or Rb) calculated with these refinements is an average distribution for a great number of cells.

3. Results and discussion

3.1. Structural rules

3.1.1. The space group and unit cell. On one hand the extinction rules were observed for $0kl$ with $h + l = 2n + 1$ and $hk0$ with $h = 2n + 1$ reflections without any violation for each $Rb_xCs_{2-x}ZnCl_4$ crystal. Therefore, the space group could be the non-centrosymmetric group $Pn2_1a$ (No 33) or the centrosymmetric group *Pnma* (No 62). Following the results of the statistics $N(Z)$ test [23], which suggests the existence of the inversion, structures were resolved in the centrosymmetric space group *Pnma*. Figure 3(a) presents the composition dependence of the lattice parameters, at room temperature. One can see that the lattice parameter b presents a continuous decrease with x while parameters a and c exhibit a discontinuity. We notice a slope break probably near $x = 1$ with a continuous variation on each side.

On the other hand, we observed that in the $K_xCs_{2-x}ZnCl_4$ crystals a few extinctions $0kl$ and $hk0$ are not verified according to the *Pnma* and $Pn2_1a$ extinction rules. These reflections are weak and their number increases with x. This release of extinctions is due to the K substitution. In order to retain maximum information, we resolved the structures in the $P2_12_12_1$ space group (extinction rules $h00, h = 2n + 1; 0k0, k = 2n + 1; 00l, l = 2n + 1$). A linear decrease in the a, b and c parameters with increasing potassium concentration can be seen in figure 3(b) ($0 \leqslant x \leqslant 1$).

3.1.2. Structure and alkaline distribution.

$Rb_xCs_{2-x}ZnCl_4$ mixed crystals. Heavy-atom coordinates from the assumed isostuctural Cs_2ZnCl_4 compound [19] were used as an initial model for the resolution of the first compound: $Rb_{0.34}Cs_{1.66}ZnCl_4$. Then, chlorine atoms were located by Fourier difference synthesis. The good evolution of the refinement allowed the introduction of rubidium in the two cationic sites. At the beginning of the multiplicity refinement, the occupancy of Cs and Rb was assumed to be equal at the A_1 and A_2 sites, but refinements gave rapid convergence ($R = 0.017$ and $R_w = 0.024$) to site occupancies zero for Rb(1) (Rb in the A_1 site) and 0.332 for Rb(2) (Rb in the A_2 site).

For the other compound, resolution and refinement were performed in a similar way, using the atomic positions of the compound having the nearest composition x.

The substitution of caesium for rubidium modifies weakly the structure of the pure Cs_2ZnCl_4 compound. At room temperature, each crystal is isostructural to the Cs_2ZnCl_4 normal phase (space group *Pnma*), so the structure of all the $Rb_xCs_{2-x}ZnCl_4$ compounds is illustrated by the projections shown in figure 1. The distribution of Cs and Rb among the two cationic sites was studied in most detail. Table 1 lists the refined occupation rate of Cs and Rb in each of the two available sites, A_1 and A_2. It is clear that the substitution is not random: Rb and Cs are not equally distributed among the two cationic sites. Rubidium atoms exhibit a higher affinity for the A_2 site and this explains the specific dependence of the lattice parameters a, b and c on the composition x (figure 3). For $0 \leqslant x < 1$, the substitution of smaller rubidium cations for caesium in the A_2 site exclusively results in a contraction of the α chain (figure 1(b)), which is solely composed of alkaline cations. This leads to an important decrease in the cell parameters a and c (figure 3(a)). For $1 < x \leqslant 2$, the rubidium cations can be located in the A_1 site which belongs to the β chain. Along the c direction, the 'width' of this chain is essentially determined by the $ZnCl_4$ tetrahedron size, which varies weakly with x (see subsubsection 3.2.3). So, the c parameter is nearly constant. On the other hand, replacement of caesium by a smaller cation allows the tetrahedra to become

Table 1. Occupation rates in the two different sites of the $Rb_xCs_{2-x}ZnCl_4$ mixed crystals.

	A_1 site		A_2 site			
Sample	Cs(1) a	Rb(1) $(1-a)$	Cs(2) b	Rb(2) $(1-b)$	$x = 2-a-b$	Chemical formula
1	1	0	0.658	0.342	0.34	$Rb_{0.34}Cs_{1.66}ZnCl_4$
2	1	0	0.462	0.538	0.54	$Rb_{0.54}Cs_{1.46}ZnCl_4$
3	1	0	0.288	0.712	0.71	$Rb_{0.71}Cs_{1.29}ZnCl_4$
4	0.889	0.111	0	1	1.11	$Rb_{1.11}Cs_{0.89}ZnCl_4$
5	0.688	0.312	0	1	1.31	$Rb_{1.31}Cs_{0.69}ZnCl_4$
6	0.406	0.594	0	1	1.59	$Rb_{1.59}Cs_{0.41}ZnCl_4$
7	0.109	0.891	0	1	1.89	$Rb_{1.89}Cs_{0.11}ZnCl_4$

Table 2. Occupation rates in the two different sites of the $K_xCs_{2-x}ZnCl_4$ mixed crystals.

	A_1 site		A_2 site			
Sample	Cs(1) a	K(1) $(1-a)$	Cs(2) b	K(2) $(1-b)$	$x = 2-a-b$	Chemical formula
$1'$	1	0	0.784	0.216	0.216	$K_{0.22}Cs_{1.78}ZnCl_4$
$2'$	1	0	0.729	0.271	0.271	$K_{0.27}Cs_{1.73}ZnCl_4$
$3'$	1	0	0.565	0.435	0.435	$K_{0.43}Cs_{1.57}ZnCl_4$
$4'$	1	0	0.379	0.621	0.621	$K_{0.62}Cs_{1.38}ZnCl_4$
$5'$	1	0	0.303	0.697	0.697	$K_{0.70}Cs_{1.30}ZnCl_4$
$6'$	1	0	0.150	0.850	0.850	$K_{0.85}Cs_{1.15}ZnCl_4$
$7'$	1	0	1	1	1	$KCsZnCl_4$

closer and causes a considerable decrease of the a parameter for $1 < x \leqslant 2$. Finally, the atomic arrangement given by the projection in figure 1(a) makes it clear that the b value is mainly determined by the tetrahedron size, so it is nearly constant for $0 \leqslant x \leqslant 2$.

$K_xCs_{2-x}ZnCl_4$ mixed crystals. Structures were resolved and refined in the same way as the compounds previously discussed. A different situation occurs in this case because the potassium introduction caused the removal of the symmetry planes and of the inversion which were present in the pure compound Cs_2ZnCl_4: a small amount ($x = 0.22$) is sufficient to change the structure of the pure compound, and these changes become more important when x increases. As an example, figure 4 shows projections of the $KCsZnCl_4$ structure along the c and b axes. They exhibit the disappearance of the symmetry planes and of the inversion. In particular, figure 4(a) shows well the loss of the m mirror perpendicular to the b axis.

The occupation rates of potassium and caesium atoms in each of the two available sites are listed in table 2. The substitution is not random. When we replace Cs by K in Cs_2ZnCl_4, we never observe K cations in the A_1 site. This leads to a limit composition $KCsZnCl_4$, in agreement with the crystal growth analysis.

The exclusive substitution in the A_1 site clarifies the evolution of the lattice parameters shown in figure 3(b). This evolution is explained in the same way as for the $Rb_xCs_{2-x}ZnCl_4$ compounds with $0 \leqslant x < 1$.

3.1.3. Site characterization. In order to explain the non-random substitution in the A_1 and A_2 sites, we have specially studied the cavities of these two sited for both the solid

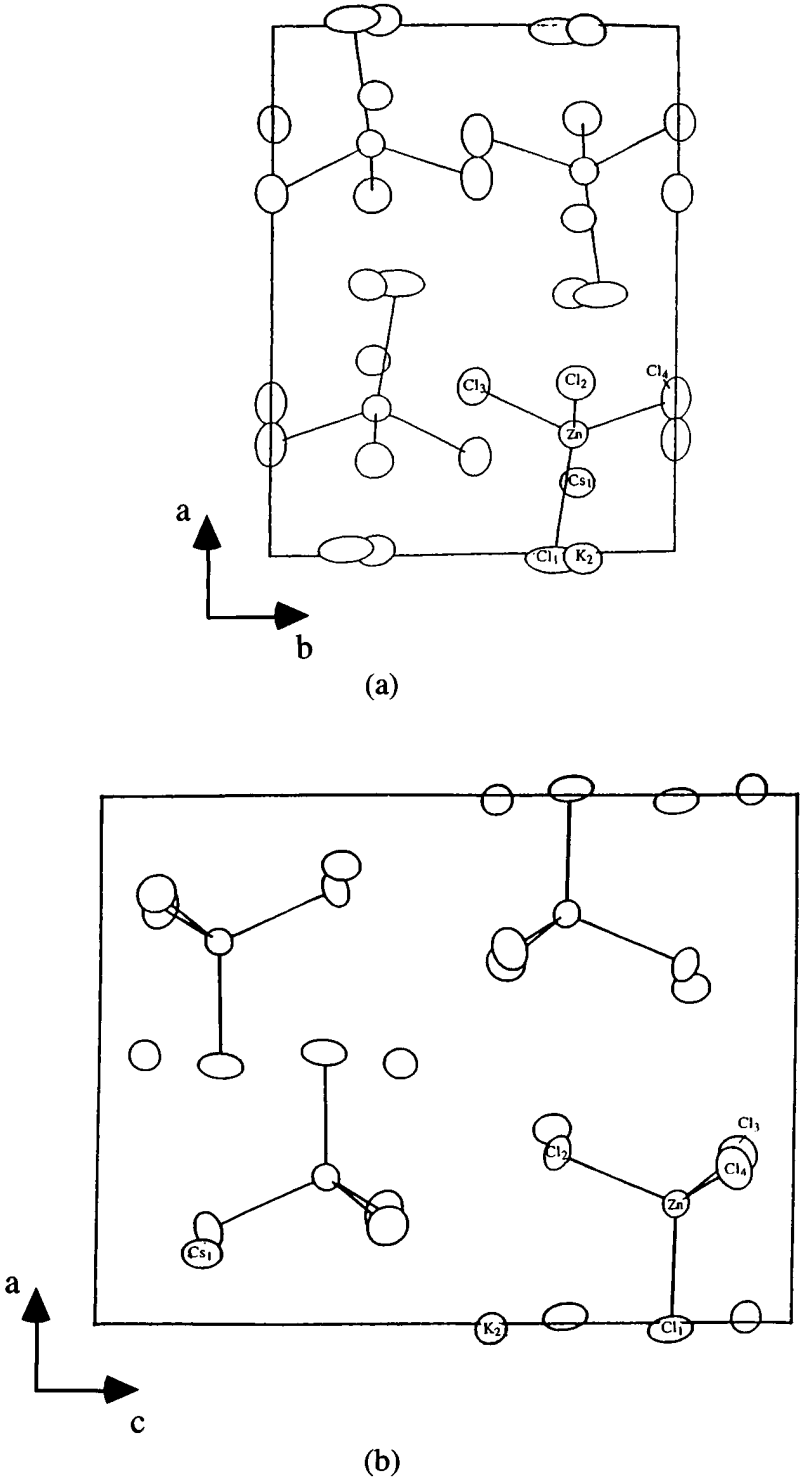

Figure 4. The crystal structure of $KCsZnCl_4$ viewed along (a) the *c* axis and (b) the *b* axis.

solutions and the pure compounds. Note that for the pure compounds the structural results are referred to [19] for Cs_2ZnCl_4, [18] for Rb_2ZnCl_4 and [13] for K_2ZnCl_4.

First, A_1 and A_2 do not have the same environment. The A_1 site has 11 first neighbours (chlorine atoms) at distances which are well superior to those observed for the A_2 site; the latter is surrounded by only nine chlorine atoms. As a consequence, since it is surrounded by more atoms, A_1 appears more spherical than A_2. So, it seems logical that the potassium and rubidium cations preferably occupy the A_2 site because they are less electropositive, and therefore less spherical, then the caesium cation.

Furthermore, we performed calculations in order to determine the cavity volume V_c of each site. For these calculations, cavities were considered as polyhedra whose vertices are the n chlorine atoms ($n = 9$ or 11) surrounding the potassium, rubidium or caesium cations. These polyhedra were divided into $2n$-4 tetrahedra, which correspond to the $2n$-4 possible choices of three of the n surrounding chlorines (a cation potassium, rubidium or caesium is the vertex).

At first, the calculations were performed using the coordinates of the surrounding chlorine atoms. The knowledge of the atomic positions allowed us to calculated the volume of each tetrahedron. The sum of these last gives the volume V_C of the cavities. Then we also calculated the volume V_{Cl} occupied by the chlorine anions inside the cavities. The Cl anions were assumed to be spherical ($r_{Cl}- = 1.81$ Å [24]). For each tetrahedron vertex (labelled i) located at the centre of a chlorine atom, the solid angle Ω_i, interior to the tetrahedron, has been determined and the total volume of chlorine inside the tetrahedra is obtained by

$$V_t = \sum_i \frac{4\pi}{3}(r_{Cl^-})^3 \frac{\Omega_i}{4\pi}.$$

Another sum leads to the total volume V_{Cl} occupied by the chlorine atoms inside each cavity. So the difference $V_c - V_{Cl}$ gives the free volume V_f which is left for the alkaline cations in each site. These calculations were performed for each solid solution and pure compound. The results are presented in figure 5. As expected, the substitution of the smaller Rb or K cation for Cs results in a more important decrease of the A_2 site volume for $0 \leqslant x \leqslant 1$ and of the A_1 site volume for $1 \leqslant x \leqslant 2$. In both cases, the A_1 site is always more expended (about +40%) than the A_2 site.

Moreover, other calculations performed with the $K_xCs_{2-x}ZnCl_4$ solid solutions and reported in a previous paper [25] indicate that the calculated electrostatic potential in both sites are different. We observe that the potential of the A_1 site is clearly flat, even though the potential of the site A_2 is a simple well.

It appears that we can start from the Cs_2ZnCl_4 pure compound and can easily substitute the Cs cation, which occupies the 'narrow' A_2 site, for the smaller Rb or K cation ($r_{Cs+} = 1.67$ Å, $r_{Rb+} = 1.48$ Å, $r_{K+} = 1.33$ Å [24]) until this site is completely filled (x varying from zero to unity). In contrast, the substitution in the A_1 site is only possible with rubidium because, in the presence of caesium, the potassium cation is too small and cannot stay in the large A_1 site, which does not present an equilibrium position.

3.2. The phase transition mechanism

3.2.1. Phase transition temperature. Calorimetric measurements of $K_xCs_{2-x}ZnCl_4$ single crystals were reported in a previous paper [25].

For the $Rb_xCs_{2-x}ZnCl_4$ crystals, a great number of heating and cooling cycles were performed between 100 and 400 K. In $Rb_{1.89}Cs_{0.11}ZnCl_4$, they show the presence of two

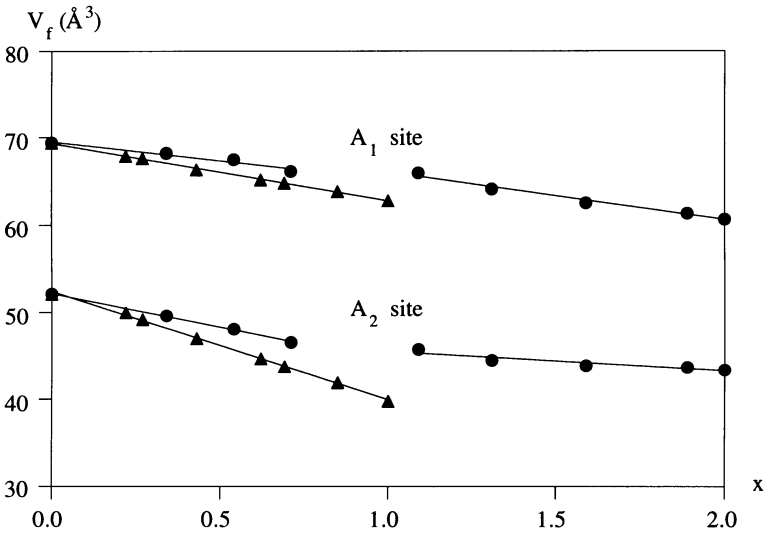

Figure 5. The composition dependence of the volumes V_f for each site in (●) the $Rb_xCs_{2-x}ZnCl_4$ mixed crystals and the $K_xCs_{2-x}ZnCl_4$ mixed crystals (▲).

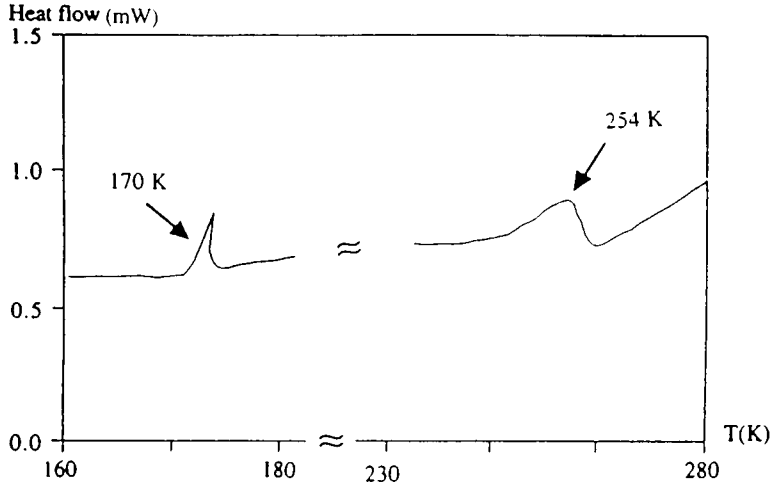

Figure 6. Heat flow curves of $Rb_{1.89}Cs_{0.11}ZnCl_4$ measured during heating.

thermal anomalies at $T = 254$ and 170 K (figure 6). Despite the rather small effect, we can suppose that the transition at 254 K is of second order while the transition at 170 K is of first order. By analogy with the pure Rb_2ZnCl_4 compound, we suggest that the first transition is an N–INC phase transition while the second is an INC–C transition leading to a ferroelectric phase.

For the other compositions, no significant thermal anomaly was observed, perhaps because of the very small effects that could not be detected.

Table 3. Anistropic thermal parameters ($Å^2$) in Rb_2ZnCl_4 at $T = 333$ K.

Atom	U_{11}	U_{22}	U_{33}	U_{12}	U_{13}	U_{23}
Zn	0.0298(5)	0.0373(5)	0.0355(5)	0	0.0005(5)	0
Cl_1	0.0158(8)	**0.095(5)**	0.050(1)	0	−0.007(1)	0
Cl_2	0.037(1)	**0.128(3)**	0.031(1)	0	−0.013(1)	0
Cl_3	0.060(1)	0.0458(9)	**0.116(2)**	0.008(1)	0.031(1)	0.038(1)
Cl_4	0.060(1)	0.0458(9)	**0.116(2)**	0.008(1)	0.031(1)	0.038(1)
Rb_1	0.0389(5)	0.0717(7)	0.119(1)	0	0.0083(57)	0
Rb_2	0.0358(4)	0.0664(6)	0.0396(5)	0	0.0013(4)	0

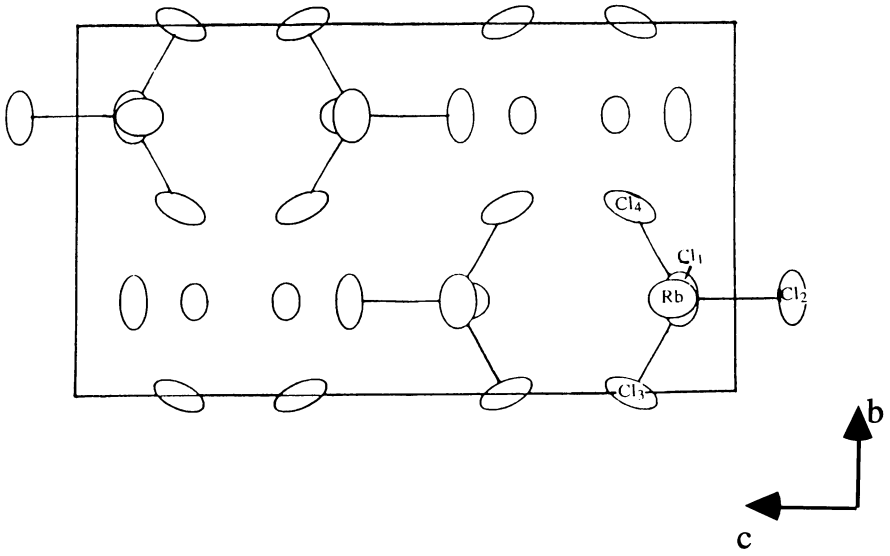

Figure 7. A (100) view of the unit cell of Rb_2ZnCl_4 at $T = 333$ K.

3.2.2. Thermal agitation of the chlorine atoms. It has been shown that the phase transition in the Rb_2ZnCl_4 and K_2ZnCl_4 compounds can be interpreted as rotation of rigid $ZnCl_4$ tetrahedra mainly around the *a* direction.

Structural data, and in particular thermal parameters, can be very useful for the prediction of these rotations and then transitions. For example, table 3 lists the anisotropic thermal parameters obtained after refinement of the Rb_2ZnCl_4 structure at $T = 333$ K (normal phase) [18]. We observe very large values of the temperature factors U_{22} (*b* direction) for the Cl_1 and Cl_2 chlorine atoms, and of U_{33} (*c* direction) for the Cl_3 and Cl_4 chlorine atoms. The projections of this compound structure along the *a* axis (figure 7) shows that these large values of the anisotropic thermal parameters in the *c* of *b* directions can be well related to the oscillations of tetrahedra along the *a* axis. These oscillations signify the static rotations which will take place at low temperatures in the incommensurate, and then in the commensurate phase.

The same abnormal large values are observed for the normal phase of K_2ZnCl_4 [13], but not in Cs_2ZnCl_4 since this latter crystal remains in the normal phase when the temperature decreases.

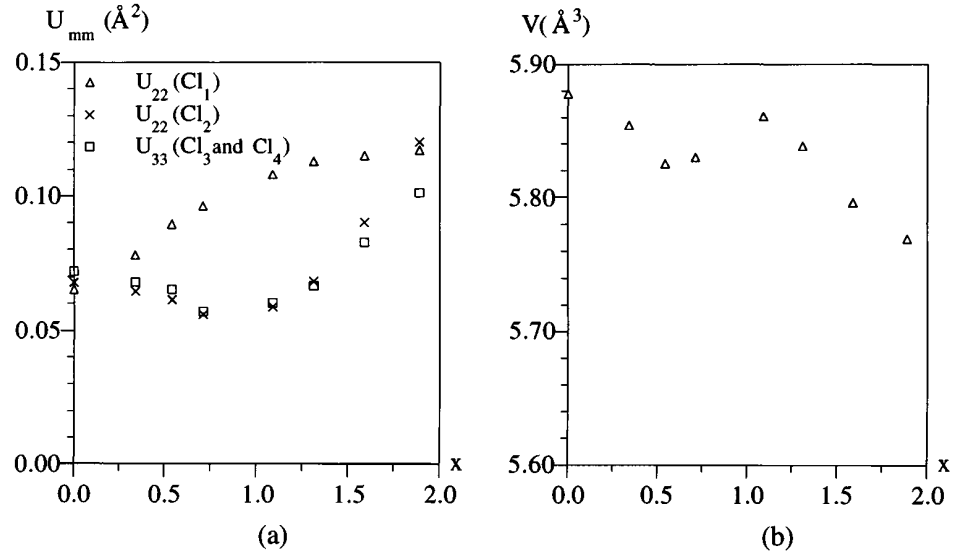

Figure 8. The composition dependence of (a) some thermal parameters and (b) the tetrahedron volumes, in $Rb_xCs_{2-x}ZnCl_4$ at 293 K.

In order to follow the evolution of these values with the substitution, we report, in figure 8(a), the dependence of several temperature factor values on x in $Rb_xCs_{2-x}ZnCl_4$. Moreover, as the presence of an instability is related to the size of the tetrahedra which can be free or compressed in the lattice, we simultaneously report, in figure 8(b), the dependence of the composition of the calculated volume of these tetrahedra (the volume is calculated as described in subsubsection 3.2.3).

When x varies from zero to unity, the temperature factors decrease slightly for the Cl_2, Cl_3 and Cl_4 chlorine atoms while they weakly increase in the case of Cl_1. In the same range of composition, the tetrahedron volume decreases slightly. This exhibits the relative stability of the structures with $x < 1$. The tetrahedra are not compressed and no phase transition is expected when temperature decreases.

On the other hand, from $x = 1$ until $x = 1.89$, the tetrahedron size drops drastically. the tetrahedra are more and more compressed and their oscillations increase rapidly, as revealed by the increasing values of the thermal parameters of each chlorine atom. We can conclude that the structures in the composition range $x > 1$ are unstable in the *Pnma* phase and suggest the phase transitions which were actually observed for compositions near $x = 2$, at lowered temperature.

The same study was made for the $K_xCs_{2-x}ZnCl_4$ crystals. Figure 9 presents the composition dependence of thermal parameters and tetrahedron size in $K_xCs_{2-x}ZnCl_4$. The results can be compared with the first part ($0 \leqslant x \leqslant 1$) of the previous figures and indicate a relative stability of the mixed compounds in the $P2_12_12_1$ space group. This was confirmed [25] by the absence of an anomaly in the calorimetric and dielectric curves for $0.22 \leqslant x \leqslant 0.85$. The $KCsZnCl_4$ compound, which is not only a limit compound but also a new definite crystal (one K cation in the A_2 site and one Cs cation in the A_1 one) is more complex. The thermal parameters of $KCsZnCl_4$ are smaller than those reported for the mixed compounds, even so, we detected a phase transition at $T = 241$ K [25].

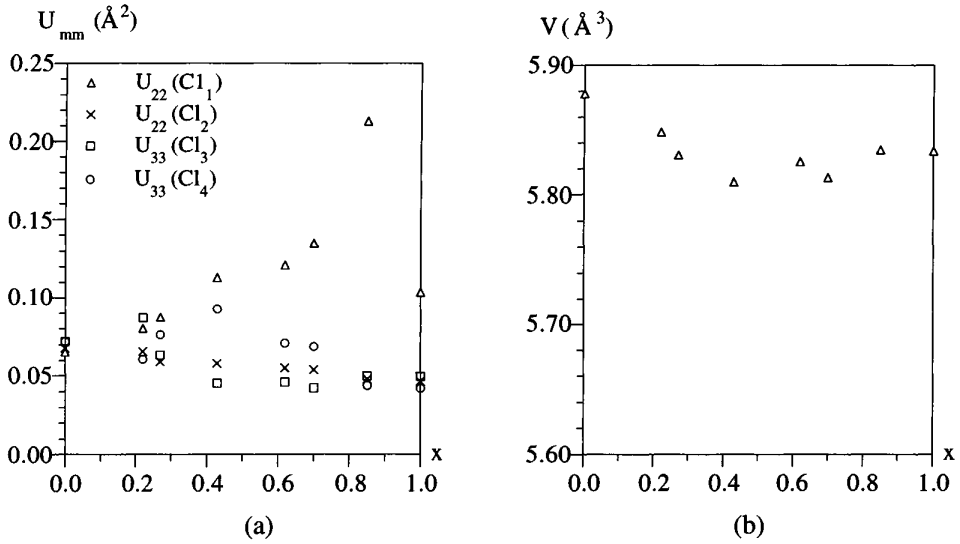

Figure 9. The composition dependence of (a) some thermal parameters and (b) the tetrahedron volumes, in $K_xCs_{2-x}ZnCl_4$ at 293 K.

3.2.3. Static deviations of $ZnCl_4$.

The distance between Zn and the barycentre B of chlorine atoms. The barycentre position of the chlorine atoms in $ZnCl_4$ is defined by the equation:

$$\vec{BCl_1} + \vec{BCl_2} + \vec{BCl_3} + \vec{BCl_4} = 0.$$

As the tetrahedron is not a regular one, Zn and B are not at the same site.

All $Rb_xCs_{2-x}ZnCl_4$ mixed crystals are refined in the *Pnma* space group. In this phase, Cl_1 and Cl_2 are in the *m* mirror (perpendicular to *b*), while Cl_3 and Cl_4 are equivalent due to this symmetry element; B and Zn are also situated in the mirror and the B–Zn length gives the anisotropy of the symmetric tetrahedron $ZnCl_4$. Figure 10 exhibits the B–Zn length, which is about 0.06 Å for almost all the crystals except for the $Rb_{1.89}Cs_{0.11}ZnCl_4$ crystal, which has a large anisotropy (d(B–Zn) = 0.20 Å). At room temperature this crystal is very near the incommensurate phase.

The $K_xCs_{2-x}ZnCl_4$ mixed crystals are refined using the $P2_12_12_1$ space group. In this phase, the $XnCl_4$ tetrahedron is not symmetric because there is nor mirror: B and Zn atoms are in general positions, and the B–Zn lengths give an idea of the tetrahedron distortion. Figure 10 shows that mixed crystals have a length (about 0.80 Å) larger than that in the pure and limit mixed crystals (Cs_2ZnCl_4, d(B–Zn) = 0.060 Å and $KCsZnCl_4$, d(B–Zn) = 0.066 Å), so the disorder of K and Cs at the A_2 site seems to increase the distortion of the $ZnCl_4$ tetrahedron.

Volume of the $ZnCl_4$ tetrahedron. Knowing the positions of the four chlorine atoms, we calculated the volume of the $ZnCl_4$ tetrahedron for both pure and mixed crystals: V is the volume for the Cs_2ZnCl_4 reference crystal ($V = 5.88$ Å^3) and $V + \Delta V$ the volume for each mixed crystal. The composition dependence of the relative contraction $-\Delta V/V$ in $Rb_xCs_{2-x}ZnCl_4$ and $K_xCs_{2-x}ZnCl_4$ is presented in figure 11.

The contraction in the $Rb_xCs_{2-x}ZnCl_4$ mixed crystals has two maxima. The first maximum ($-\Delta V/V = 0.018$) occurs when the A_1 site is occupied only by caesium

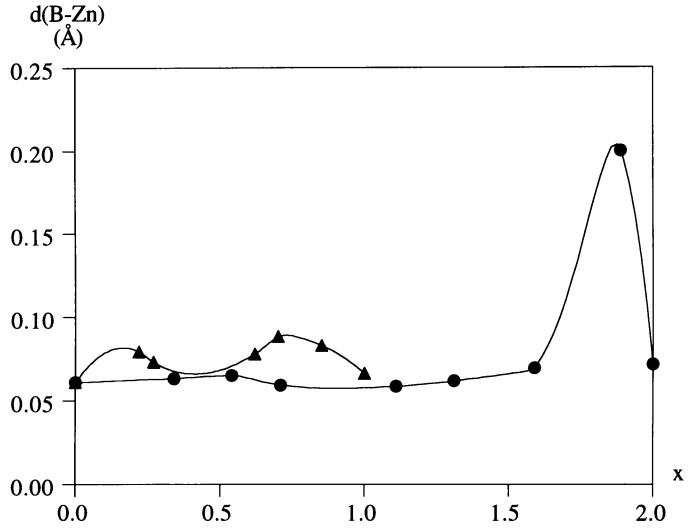

Figure 10. B–Zn length versus x in the $Rb_xCs_{2-x}ZnCl_4$ (●) and the $K_xCs_{2-x}ZnCl_4$ mixed crystals (▲).

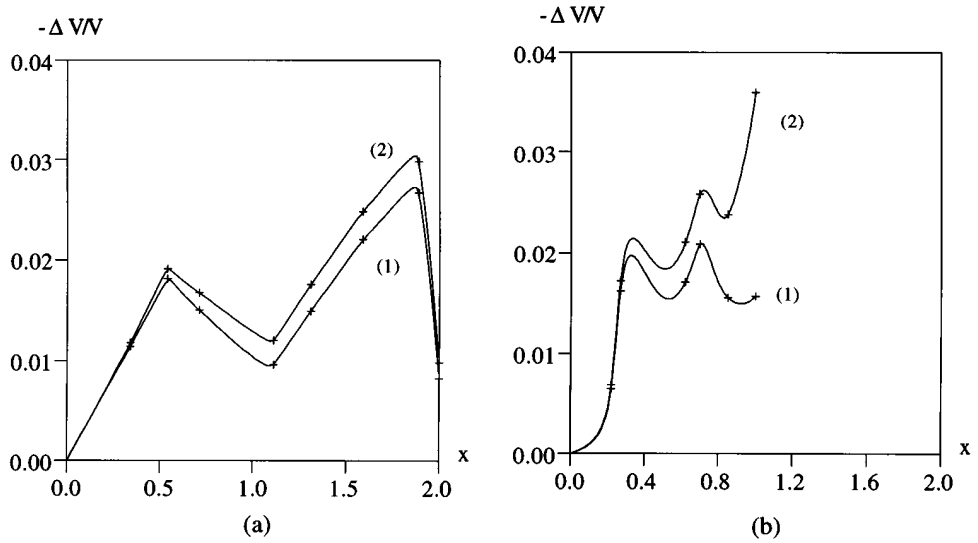

Figure 11. The composition dependence of the contraction from the atomic positions of the chlorine atoms (without approximation) (1) and from the trace of the distorsion symmetric matrix (first-order approximation) (2). (a) relative to the $Rb_xCs_{2-x}ZnCl_4$ compounds and (b) referred to the $K_xCs_{2-x}ZnCl_4$ compounds.

and the A_2 site is filled by 50% caesium and 50% rubidium. The second maximum ($-\Delta V/V = 0.027$) corresponds to the composition $x = 1.89$ for which the crystal is near the incommensurate phase. We also observe that the contraction is the smallest for the pure Rb_2ZnCl_4 crystal ($-\Delta V/V = 0.008$) and for the $Rb_{1.11}Cs_{0.89}ZnCl_4$ crystal ($-\Delta V/V = 0.009$). This latter composition has approximatively one caesium cation in the A_1 site and one rubidium cation in the A_2 site.

In the $K_xCs_{2-x}ZnCl_4$ mixed crystals, the contraction is nearly constant and about $-\Delta V/V = 0.017$ when $0.27 \leqslant x \leqslant 1$. The tetrahedron volume is smaller in $KCsZnCl_4$ ($-\Delta V/V = 0.016$) than in $Rb_{1.11}Cs_{0.89}ZnCl_4$ ($-\Delta V/V = 0.009$) because in mixed crystals, with approximately one Cs in the A_1 site and one Rb (or K) in the A_2 site, the K atoms compress the tetrahedra more than the Rb atoms.

In most cases, the contraction calculation in the first-order approximation gives roughly the same results as the calculation without approximation. However, as explained below, for the $K_xCs_{2-x}ZnCl_4$ mixed crystals with $0.7 \leqslant x \leqslant 1$, the first-order approximation is not sufficient.

The first-order approximation: the displacement tensor. When we compare the pure Cs_2ZnCl_4 crystal and the mixed crystals, we assume that the problem of specifying the state of rotation and the strain of $ZnCl_4$ is the same as the change of the solid body shape subjected to stress.

We fix the origin in space [26] and study the displacements u_i of the solid body points with coordinates x^j. For small displacements, the variation of x with the positions is used to define nine tensor components:

$$T_{ij} = \partial u_i/\partial x^j \qquad (i, j = 1, 2, 3)$$

or in the Einstein notation

$$\Delta u_i = T_{ij}\ \Delta x^j \quad \text{(sum over } j\text{)}.$$

To completely determine all nine components T_{ij} it is necessary to know three different displacements $\Delta\boldsymbol{u}$ for three different vectors $\Delta\boldsymbol{x}$ with the origin at the same point. In our case, the choice of the barycentre of chlorine atoms as the vector origin permits us to calculate the nine components T_{ij} by using position data of three arbitrary chlorine atoms among the four.

Similarly, in the case of $ZnCl_4$, the common origin is the barycentre of the four Cl atoms in the pure Cs_2ZnCl_4 compound and we choose the four vectors $\vec{BCl}_i$. In mixed crystals these vectors become $\vec{B'Cl}'_i$, with B′ the barycentre of the four chlorines Cl'_i. The small displacement of $\vec{BCl}_i$ is the vector $\vec{B'Cl}'_i - \vec{BCl}_i$, which gives the change of the $\vec{BCl}_i$ distance in pure and mixed crystals.

We introduce the following notation for the distances ($\boldsymbol{p}, \boldsymbol{q}, \boldsymbol{r}, \boldsymbol{s}$) between the chlorine atoms and their barycentre in pure Cs_2ZnCl_4 and for the changes of the distances ($\boldsymbol{u}, \boldsymbol{v}, \boldsymbol{w}, \boldsymbol{t}$) in mixed crystals:

$$\begin{aligned}
\boldsymbol{p} &= \vec{BCl}_1 \qquad & \boldsymbol{u} &= \vec{BCl}_1 - \vec{B'Cl}'_1\\
\boldsymbol{q} &= \vec{BCl}_2 \qquad & \boldsymbol{v} &= \vec{BCl}_2 - \vec{B'Cl}'_2\\
\boldsymbol{r} &= \vec{BCl}_3 \qquad & \boldsymbol{w} &= \vec{BCl}_3 - \vec{B'Cl}'_3\\
\boldsymbol{s} &= \vec{BCl}_4 \qquad & \boldsymbol{t} &= \vec{BCl}_4 - \vec{B'Cl}'_4
\end{aligned}$$

The definition of the barycentres B (pure crystal) and B′ (mixed crystal) gives the following equations:

$$\boldsymbol{p} + \boldsymbol{q} + \boldsymbol{r} + \boldsymbol{s} = \boldsymbol{0} \qquad \boldsymbol{u} + \boldsymbol{v} + \boldsymbol{w} + \boldsymbol{t} = \boldsymbol{0}.$$

In the first-order linear approximation, we introduce the nine components T_{ij} of the second-rank tensor $\overline{\overline{T}}$ to express the projections (u_i, v_i, w_i, t_i on the axis, $i = 1, 2, 3, 1$ on $\boldsymbol{a}$, 2 on $\boldsymbol{b}$, 3 on $\boldsymbol{c}$) of the distance changes as functions of the projections of the lengths (p^j, q^j, r^j, s^j on the axis, $j = 1, 2, 3$).

We write

$$u_i = T_{ij}\,p^j \text{ with sum on } j \text{ (Einstein notation)}$$
$$v_i = T_{ij}q^j \text{ with sum on } j \text{ (Einstein notation)}$$
$$w_i = T_{ij}r^j \text{ with sum on } j \text{ (Einstein notation)}$$

and

$$t_i = T_{ij}s^j \text{ as a verification.}$$

We use the following matrix notation:

$$\begin{pmatrix} u_1 & v_1 & w_1 \\ u_2 & v_2 & w_2 \\ u_3 & v_3 & w_3 \end{pmatrix} = \begin{pmatrix} T_{11} & T_{12} & T_{13} \\ T_{21} & T_{22} & T_{23} \\ T_{31} & T_{32} & T_{33} \end{pmatrix} \begin{pmatrix} p^1 & q^1 & r^1 \\ p^2 & q^2 & r^2 \\ p^3 & q^3 & r^3 \end{pmatrix}$$

or

$$\mathbf{U} = \mathbf{TP}$$

with $\mathbf{T}$ the matrix which represents the $\overline{\overline{T}}$ tensor, $\mathbf{U}$ the matrix of length changes and $\mathbf{P}$ the matrix of lengths.

By calculating the $\mathbf{P}^{-1}$ inverse of matrix $\mathbf{P}$, we obtain the $\mathbf{T}$ matrix:

$$\mathbf{T} = \mathbf{UP}^{-1}.$$

The nine T_{ij} components were calculated and verificated with t_i and s^j for all mixed crystals. The symmetric part $S_{ij} = (T_{ij} + T_{ji})/2$ gives the distortion of the tetrahedron while the antisymmetric part $A_{ij} = (T_{ij} - T_{ji})/2$ gives its rotation.

The first-order linear approximation is good if (u_i, v_i, w_i) are small compared to (p_j, q_j, r_j). In this case, the relative change of the tetrahedron volume is approximately

$$\Delta V/V \cong S_{11} + S_{22} + S_{33} \cong T_{11} + T_{22} + T_{33} \cong \mathrm{Tr}\,\mathbf{T}.$$

It is equal to the trace of the displacement matrix, which is the same as the trace of the distortion symmetric matrix. This approximation proves to be good in all cases except for the $K_xCs_{2-x}ZnCl_4$ mixed crystal with $0.7 \leqslant x < 1$: the changes of the $B'\vec{Cl}_i - B\vec{Cl}_i$ lengths compared to the $B\vec{Cl}_i$ distances are not small enough.

Rotation of the $ZnCl_4$ tetrahedron. The comparison of the tetrahedron in Cs_2ZnCl_4 and in mixed crystals shows an $\boldsymbol{\omega}$ rotation which is defined by the three projections (ω_1, ω_2, ω_3) on the three axes ($\boldsymbol{a}$, $\boldsymbol{b}$ and $\boldsymbol{c}$). These projections are related to the antisymmetric part of the displacement tensor $\overline{\overline{T}}$ by

$$\omega_1 = A_{23} \qquad \omega_2 = A_{31} \qquad \omega_3 = A_{12}.$$

$|\boldsymbol{\omega}| = (180/\pi)[A_{23}^2 + A_{31}^2 + A_{12}^2]^{1/2}$ is the rotation modulus in degrees and $\alpha_i = \omega_i/|\boldsymbol{\omega}|$ ($i = 1, 2, 3$) the director cosines of the rotation vector.

The results for the two kinds of mixed crystal are shown in figure 12.

For the $Rb_xCs_{2-x}ZnCl_4$ crystals, the $\boldsymbol{\omega}$ vector is parallel to the $\boldsymbol{b}$ axis. At first, $|\boldsymbol{\omega}|$ increases with increasing x, with a maximum value of $3°15'$ at $x = 1.89$, then decreases until $2°44'$ at $x = 2$. It is interesting to note that this behaviour is similar to the dependence of the thermal parameter $U_{22}(Cl_1)$ on x (figure 8(a)).

For the $K_xCs_{2-x}ZnCl_4$ crystals, the $\boldsymbol{\omega}$ vector is not along the $\boldsymbol{b}$ axis, and ω_1 and ω_3 are not equal to zero. The $|\boldsymbol{\omega}\alpha_2|$ projection as function of x, given by figure 12(d), shows that the rotation around the $\boldsymbol{b}$ axis is proportional to the concentration x of potassium. On the other hand, the modulus $|\boldsymbol{\omega}|$ increases rapidly with x and once again the curve looks like the $U_{22}(Cl_1)$ thermal agitation curve (figure 8(b)).

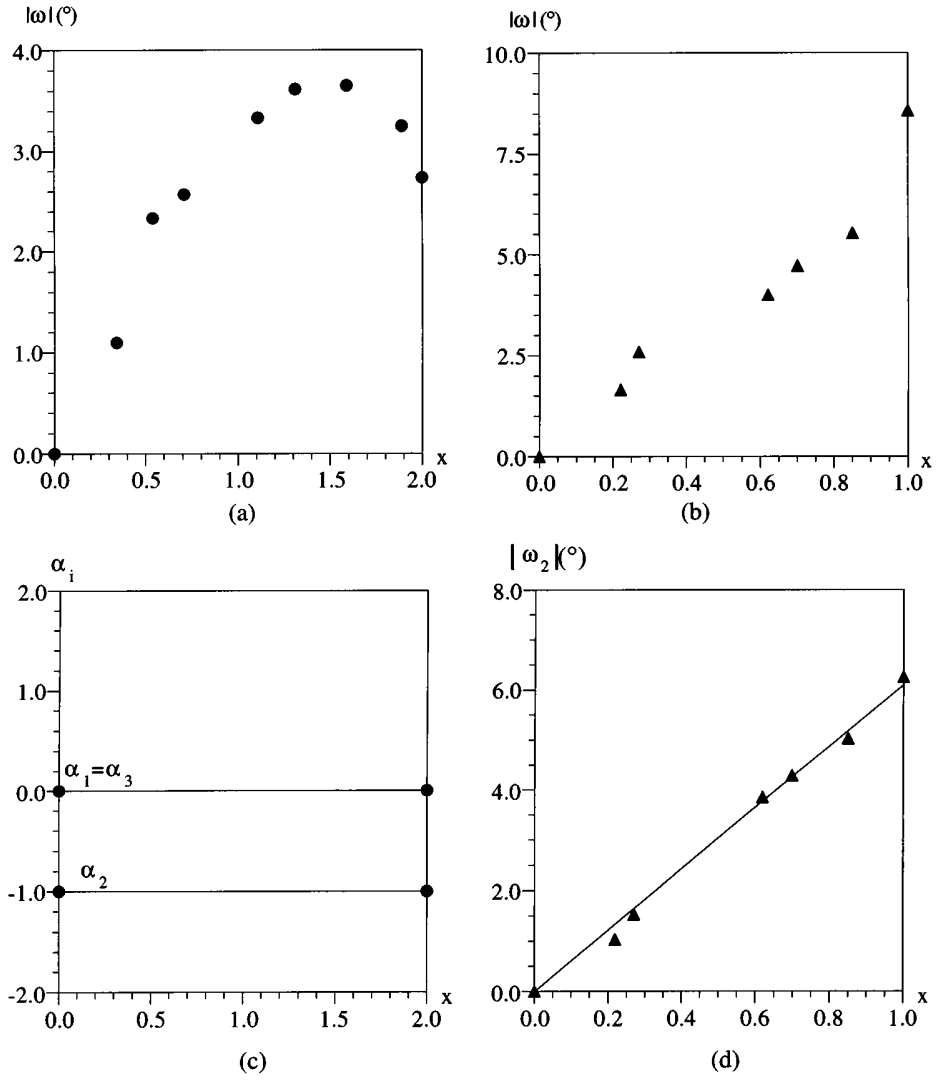

Figure 12. (a) Rotation vector modulus $|\omega|$ versus x in $Rb_xCs_{2-x}ZnCl_4$; (b) the same in $K_xCs_{2-x}ZnCl_4$; (c) director cosines α_1, α_2 and α_3 of the rotation vector in $Rb_xCs_{2-x}ZnCl_4$; (d) projection of the ω vector, on the b axis, in $K_xCs_{2-x}ZnCl_4$.

Distortion of the tetrahedron. The three $S_{ii}(i = 1, 2, 3)$ components of the symmetric matrix **S** are related to the relative dilatation (or contraction) of the lengths along the three axes $\boldsymbol{a}$, $\boldsymbol{b}$ and $\boldsymbol{c}$. We see the composition dependence of these components in the two kinds of mixed crystal in figure 13(a) and (b).

We have seen that the cell parameter $\boldsymbol{b}$ is independent of the amount x of Rb (or K) in the crystals. For exactly the same reason, S_{22} is nearly zero in all mixed crystals, i.e., the length do not change along the b axis.

The contraction in the a direction in $K_xCs_{2-x}ZnCl_4$ increases with x when the cell parameter $\boldsymbol{a}$ decreases, and this contraction is the largest ($S_{11} = -0.029$) for the limit crystal $KCsZnCl_4$. In the $Rb_xCs_{2-x}ZnCl_4$ crystals, the contraction is maximal for $x = 0.59$ and

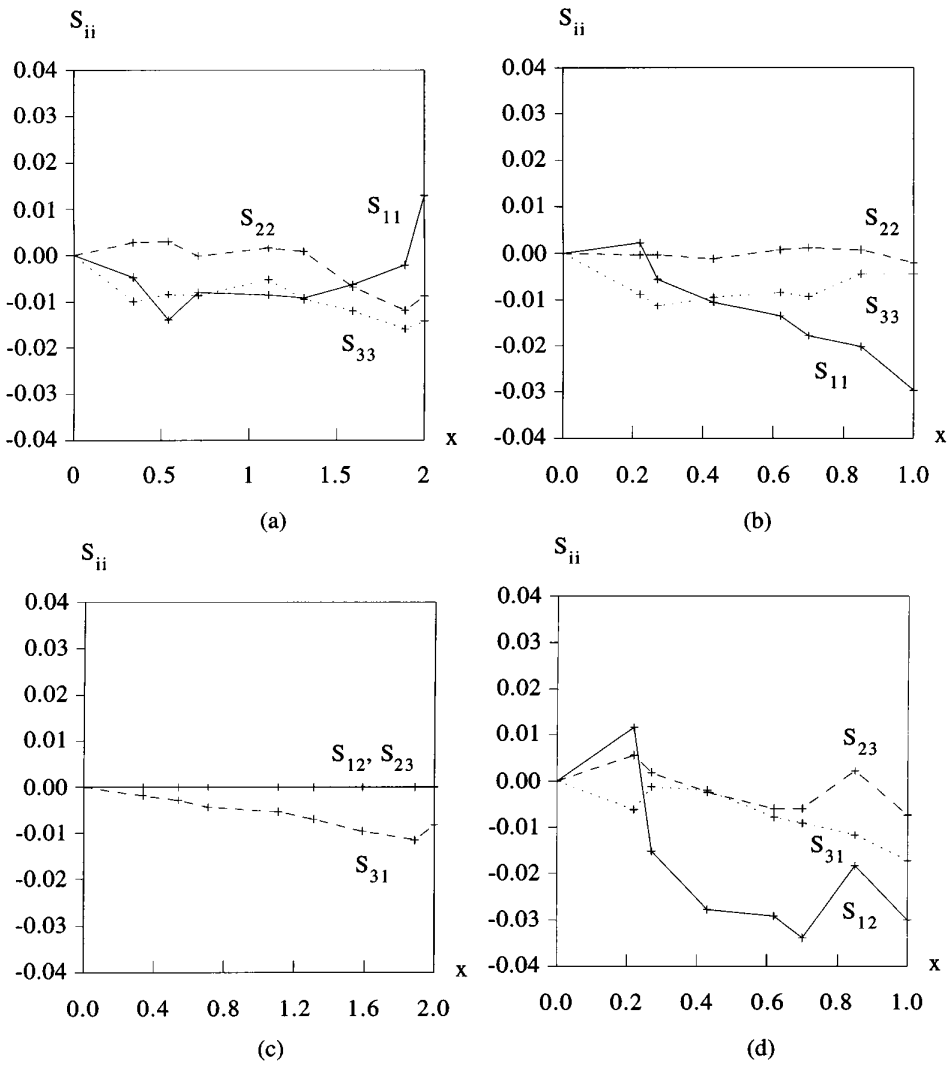

Figure 13. Contraction and dilatation of $ZnCl_4$ along $\boldsymbol{a}(S_{11})$, $\boldsymbol{b}(S_{22})$ and $\boldsymbol{c}(S_{33})$ for (a) $Rb_xCs_{2-x}ZnCl_4$ and (b) $K_xCs_{2-x}ZnCl_4$. Shearing of $ZnCl_4$: S_{23}, S_{31} and S_{12} for (c) $Rb_xCs_{2-x}ZnCl_4$ and (d) $K_xCs_{2-x}ZnCl_4$.

there is a dilatation for the pure crystal ($x = 2$), which is very near to the incommensurate phase with a modulation vector along the $\boldsymbol{a}$ axis.

Along the c axis, the value of the contraction S_{33} is about -0.01 for all mixed crystals and does not vary significantly.

The three components S_{ij} ($i \neq j$) of the symmetric matrix $\mathbf{S}$ are related to the shearing of the tetrahedron: S_{12} in the (001) plane, S_{23} in the (100) plane and S_{31} in the (010) plane. They are presented in figure 13(c) and (d).

We observe no shearing in the (001) and (100) planes for the $Rb_xCs_{2-x}ZnCl_4$ crystals, whereas the absolute value of the shearing in the (010) plane increases with x. The $\boldsymbol{b}$ axis becomes the ferroelectric axis at low temperature in Rb_2ZnCl_4 crystals.

The three shearings exist in $K_xCs_{2-x}ZnCl_4$ crystals and vary in a complicated manner with x; the largest values correspond to the $KCsZnCl_4$ limit crystal. This fact may explain why it is impossible to grow crystals with $x > 1$.

4. Conclusion

The crystal growth and crystallographic study of $K_xCs_{2-x}ZnCl_4$ and $Rb_xCs_{2-x}ZnCl_4$ solid solutions explains the possibility of phase transitions and the existence of a limit crystal $KCsZnCl_4$.

It would be interesting to complete these results by growing $K_xCs_{2-x}ZnCl_4$ solid solutions from melt compounds and obtaining crystallographic data at higher temperature. The thermal agitation and the cell volume would be larger and the contractions and shearings of the $ZnCl_4$ tetrahedra would perhaps permit us to obtain solid solutions with $1 < x < 2$ in the *Pnma* phase, like K_2ZnCl_4 at $T > 553$ K.

It would be also important to obtain potassium solid solution crystals with $0 < x < 0.22$ to understand how the *Pnma* phase with $x = 0$ and the $P2_12_12_1$ phase with $x = 0.22$ can exist at room temperature. The explanation is left for further studies.

References

[1] Haga H, Onodera A and Shrizaki Y 1992 *Ferroelectrics* **125** 123
[2] Gesi K and Iizumi M 1984 *J. Phys. Soc. Japan* **53** 4271
[3] Gesi K 1979 *J. Phys. Soc. Japan* **45** 1431
[4] Gesi K 1990 *J. Phys. Soc. Japan* **59** 416
[5] Flërov I N and Kot L A 1981 *Sov. Phys.–Solid State* **23** 1415
[6] Sawada S, Shiroishi Y, Yamamoto A, Takashige M and Matsuo M 1977 *J. Phys. Soc. Japan* **43** 2099
[7] Godefroy G, Jannot N, Dumas C and Janovec V 1988 *Ferroelectrics* **87** 233
[8] Noiret I, Hedoux A, Guinet Y and Foulon M 1993 *Europhys. Lett.* **22** 265
[9] Quilichini M, Dvorak V and Boutrouille P 1991 *J. Physique* **I** 1321
[10] Francke E, Le Postollec M, Mathieu J P and Poulet H 1980 *Solid State Commun.* **33** 155
[11] Wada M, Sawada A and Ishibashi Y 1981 *J. Phys. Soc. Japan* **50** 531
[12] Quilichini M 1987 *Incommensurate Crystals, Liquid Crystals and Quasi-Crystals (NATO ASI series 166)* (New York: Plenum) p 127
[13] Quilichini M and Heger G 1986 *10th Eur. Crystallographic Meeting (Wroclaw, 1986)*
[14] Quilichini M, Heger G and Schweiss P 1988 *Ferroelectrics* **79** 117
[15] Mickail I and Peters K 1979 *Acta Crystallogr.* B **35** 1200
[16] Quilichini M and Pannetier J 1983 *Acta. Crystallogr.* B **39** 657
[17] Hedoux A, Grebille D, Jaud J and Godefroy G 1989 *Acta. Crystallogr.* B **45** 370
[18] Kolinsky C 1994 *Thèse de Doctorat.* Université de Bourgogne
[19] Puget R, Jannin M, Perret R, Godefroy L and Godefroy G 1990 *Ferroelectrics* **107** 229
[20] Etxebarria I, Perez-Mato J M and Madriaga G 1992 *Phys. Rev.* B **46** 2764
[21] Arend H, Perret R, Wüest H and Kerkoc P 1986 *J. Crystal Growth* **74** 321
[22] 1990 *MolEN* (Delft: Enraf–Nonius)
[23] Howells E R, Phillips D C and Rogers D 1950 *Acta Crystallogr.* **3** 210
[24] Shannon R D and Prewitt C T 1969 *Acta Crystallogr.* B **25** 925
[25] Kolinsky C, Jannin M and Puget R 1994 *Ferroelectr. Lett.* **17** 13–20
[26] Nye J F 1957 *Physical Properties of Crystals* (Oxford University Press) p 98